SCIENCE CHINA Materials ARTICLES

mater.scichina.com link.springer.com

Published online 15 March 2018 | https://doi.org/10.1007/s40843-017-9229-x
Sci China Mater 2018, 61(8): 1033–1039

$PbCrO_4$ yellow-pigment nanorods: An efficient and stable visible-light-active photocatalyst for O_2 evolution and photodegradation

Guo-Qiang Zhang[1], Guoshuai Liu[2], Yangsen Xu[1], Jianhua Yang[3], Ying Li[1], Xiaojuan Sun[4*], Wei Chen[5] and Chen-Liang Su[1*]

ABSTRACT **Here, $PbCrO_4$ nanorods, a commonly used and low-cost yellow pigment, was synthesized *via* a simple precipitation reaction and can serve as a highly efficient oxygen production and photodegradation photocatalyst. The obtained $PbCrO_4$ nanorods exhibit excellent stability and photocatalytic performance for O_2 evolution from water. The production rate is approximately 314.0 μmol h^{-1} g^{-1} under visible light, and the quantum efficiency is approximately 2.16% at 420±10 nm and 0.05% at 600±10 nm. In addition, the $PbCrO_4$ shows good degradation performance for methylene blue, methyl blue, methyl orange and phenol under visible-light irradiation. These results indicate that it is potential to fabricate an effective, robust $PbCrO_4$ photocatalyst by transforming heavy-metal pollutants Pb(II) and Cr(VI) into a highly efficient O_2 evolution and photodegradation material. This strategy which uses pollutant to produce clean energy and degrade contaminants is completely green and environmentally benign, and thus could be a promising way for practical environmental applications.**

Keywords: O_2 evolution, pollutant, $PbCrO_4$ nanorods, visible-light-active, photocatalyst

INTRODUCTION

Photocatalytic water splitting is one of the most promising approaches to address energy and environmental issues [1–3]. Water splitting can be separated into two half reactions, namely, hydrogen evolution and oxygen evolution. The generation of H_2 by a photocatalyst has been heavily researched over the past several years, and the generation rates have been significantly improved. However, the O_2 generation reaction (water oxidation) is stilll difficult due to the multiple step reactions that involve four electrons with low reaction rate of about 5 orders of magnitude slower than that of the H_2 evolution. Therefore, O_2 evolution remains the major obstacle for the overall water-splitting reaction [4–6]. The basic requirement in O_2 generation is that the valence band of the photocatalyst must be more positive than the oxidation potential of H_2O to O_2 (1.23 V *versus* normal hydrogen electrode (NHE), pH=0). Furthermore, a significant overpotential is required to excite four electrons. Although a variety of materials have been developed over the past few decades for this purpose, very few materials reported can directly oxidize water into O_2 under visible-light illumination [7].

Monoclinic bismuth vanadate ($BiVO_4$), which has a relatively narrow bandgap of ~2.4 eV and highly positive valence band edge of 2.86 V *versus* NHE, is a low-cost, photostable photocatalyst that has been widely used in solar energy conversion. However, the low mobility and the high recombination rates of the photogenerated charge carriers in $BiVO_4$ usually result in a poor photocatalytic activity, which has seriously hampered its practical applications, especially for photocatalytic O_2 evolution [8,9]. Recently, silver orthophosphate (Ag_3PO_4)

[1] SZU-NUS Collaborative Innovation Center for Optoelectronic Science & Technology, International Collaborative Laboratory of 2D Materials for Optoelectronics Science and Technology of Ministry of Education, College of Optoelectronic Engineering, Shenzhen University, Shenzhen 518060, China
[2] State Key Laboratory of Urban Water Resource and Environment, School of Environment, Harbin Institute of Technology, Harbin 150090, China
[3] College of Physical Science and Technology, Central China Normal University, Wuhan 430079, China
[4] State Key Laboratory of Luminescence and Applications, Changchun Institute of Optics, Fine Mechanics and Physics, Changchun 130033, China
[5] Department of Chemistry, National University of Singapore, Singapore 117543, Singapore
* Corresponding authors (emails: sunxj@ciomp.ac.cn (Sun X); chmsuc@szu.edu.cn (Su CL))

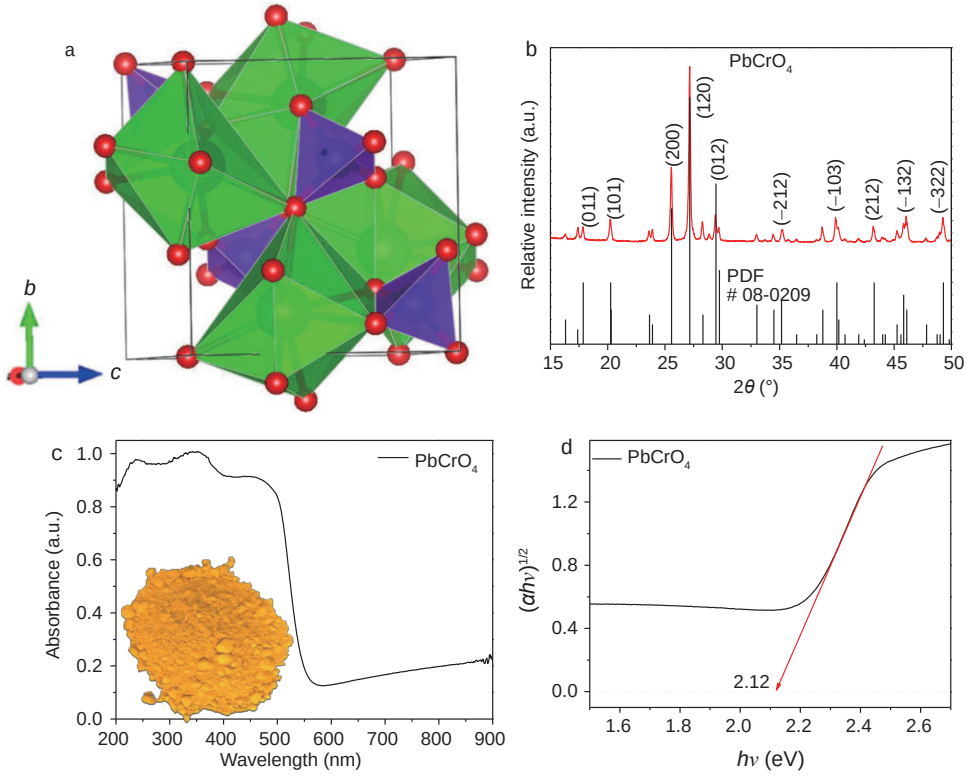

Figure 1 The crystal structure (Pb, green; Cr, purple; O, red) of $PbCrO_4$ (a). The XRD pattern (b), DRS UV-vis spectrum (c), optical image (inset of c) and Tauc plot of the transformed Kubelka-Munk function *versus* the energy (d) of the $PbCrO_4$ nanorods.

has been reported to be one of the few materials that exhibit an excellent visible-light-driven photooxidative capability for O_2 evolution from water, but Ag_3PO_4 is unstable under light irradiation and suffers from photocorrosion as a result of its self-reduction to silver by the photogenerated electrons [7,10,11]. In addition, the noble metallic composition may limit practical applications. Other O_2 evolution photocatalysts, such as TaON [12], Ta_3N_5 [13], Fe_2O_3 [14] and WO_3 [15], either are unstable under illumination or have weak photocatalytic performances. Developing highly efficient, low-cost and stable visible-light-active photocatalysts for O_2 evolution from water is a challenge.

Lead chromate ($PbCrO_4$), one of the most commonly used inorganic yellow pigments in plastics, coatings and paints, could be a good visible-light-active photocatalyst due to its excellent photostability, thermostability, easy preparation and low cost [16–18]. Herein, using a simple precipitation reaction, we transformed heavy-metal Pb(II) and Cr(VI) pollutants into the yellow pigment, $PbCrO_4$, as a stable and efficient visible-light-active photocatalyst for O_2 evolution from water with negligible pollutant residues during the photocatalytic reaction. In addition, $PbCrO_4$ has a good decomposition performance for methylene blue, methyl blue, methyl orange and phenol under visible-light irradiation. This novel and efficient photocatalyst may result in breakthroughs for the overall water-splitting reaction and specially for the reuse of pollutants containing Pb(II) and Cr(VI).

RESULTS AND DISCUSSION

The $PbCrO_4$ nanorods were synthesized by a precipitation reaction of $Pb(NO_3)_2$ and Na_2CrO_4 solutions (see Supplementary information for detail). The crystal structure and unit cell of $PbCrO_4$ (a = 7.12 Å, b = 7.44 Å, c = 6.8 Å; α = 90.0°, β = 102.4°, γ = 90.0°) are shown in Fig. 1a. The corner-connected PbO_9 twisted enneahedron and CrO_4 tetrahedron are alternately arranged in the crystal structure. The X-ray diffraction pattern (XRD) of the as-synthesized $PbCrO_4$ (Fig. 1b) exhibits a typical monoclinic phase with diffraction peaks at 17.87°, 20.31°, 25.58°, 27.17°, 29.46°, 35.18°, 40.00°, 43.25°, 45.84° and 49.30°, which are related to the (011), (101), (200), (120), (012), (−212), (−103), (212), (−132) and (−322) facets of $PbCrO_4$ (JCPDS No. 08-0209). The energy dispersive X-ray analysis (EDX) spectrum (Fig. S1) shows the molar ratio of

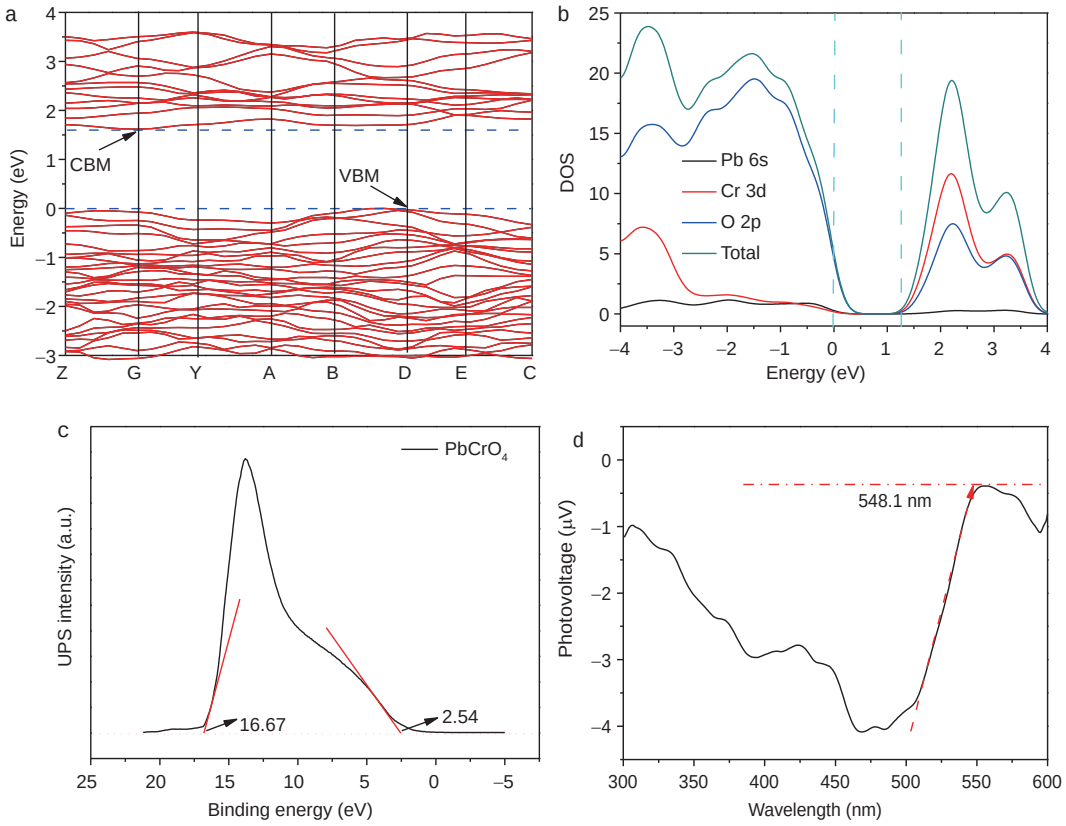

Figure 2 The calculated electronic band structures (a), DOS (b), UPS (c) and SPS (d) of the $PbCrO_4$ nanorods.

Pb, Cr and O is close to 1:1:4, indicating stoichiometric $PbCrO_4$ was successfully prepared. Diffuse reflectance UV-vis spectroscopy (DRS) was used to evaluate the absorption region of $PbCrO_4$, as presented in Fig. 1c. The deep yellow powders (Inset of Fig. 1c) have a strong absorption band in the visible-light region. The band gap of $PbCrO_4$ can be calculated to be 2.12 eV from the Tauc plot (Fig. 1d).

To better understand the electronic structure of $PbCrO_4$, we conducted density functional theory (DFT) calculations. Fig. 2a shows the calculated band structure of $PbCrO_4$ with an indirect band gap of 1.62 eV at the D and G point, which is 0.50 eV smaller than the experimental value (2.12 eV) due to the well-known standard DFT band gap underestimation. The density of state (DOS) calculation (Fig. 2b) indicates that the valance band maximum (VBM) of $PbCrO_4$ originates from the O 2p state, and the conduction band minimum (CBM) mainly originates from Cr 3d. The Pb 6s state has a relatively less contribution to the conduction band. Ultraviolet photoelectron spectroscopy (UPS) was used to determine the valence band energy (E_{VB}) of $PbCrO_4$ (Fig. 2c), which is 2.65 V *versus* the reversible hydrogen electrode (RHE) and matches the calculated E_{VB} (2.57 V *versus* the RHE) from the empirical equation (Table S1). Because the E_{VB} value is 1.42 and 0.95 V higher than the potentials of O_2/H_2O (1.23 V) and $OH/^{\cdot}OH$ (1.70 V), $PbCrO_4$ may have photocatalytic activity for O_2 evolution from water splitting and $^{\cdot}OH$ radical generation. The conduction band energy (E_{CB}) is approximately 0.53 V *versus* the RHE based on E_{VB}–E_g. Surface photovoltage spectroscopy (SPS) is a powerful tool to characterize the charge separation and the photoelectric response on the nanoscale [19]. As shown in Fig. 2d, SPS shows an active negative surface photovoltage (SPV) response, indicating $PbCrO_4$ is a p-type semiconductor [19]. The SPV response reaches 548.1 nm, which agrees with the solid $PbCrO_4$ powder absorption (Fig. 1c). Furthermore, the strong SPV response illustrates that the generated carriers can efficiently separate and rapidly migrate to the surface, indicating $PbCrO_4$ may have a good photocatalytic performance.

The field emission scanning electron microscopy (FE-SEM) images (Fig. 3a, b) and low-resolution transmission

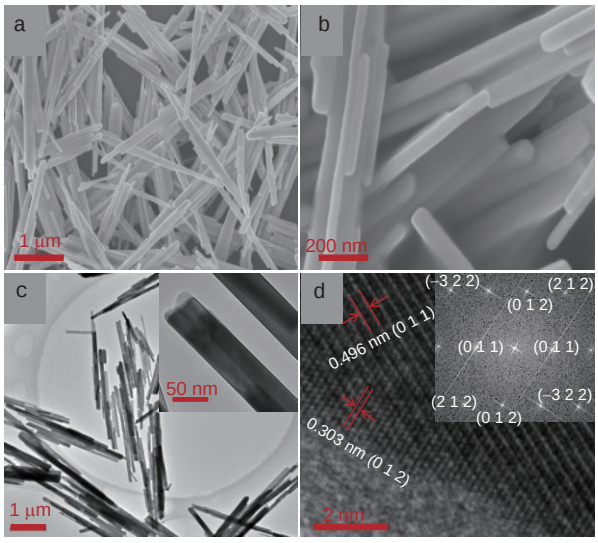

Figure 3 The FE-SEM images (a, b), low-resolution TEM image (c) and HR-TEM image (d) of the $PbCrO_4$ nanorods.

electron microscopy (TEM) images (Fig. 3c and inset) show the $PbCrO_4$ is single-crystal nanorods with 1–5 μm in length and 50–100 nm in diameter. The characteristic lattice fringe spacing of monoclinic phase $PbCrO_4$, (011) and (012), is 0.496 and 0.303 nm, respectively, observed from the high resolution TEM (HR-TEM) images (Fig. 3d). In order to interpret the synthetic mechanism of nanorod-like $PbCrO_4$, we further characterized the morphology of $PbCrO_4$ with SEM, as the reaction time prolonged. As shown in Fig. S2, the $PbCrO_4$ prepared at 180 min was obviously longer than that of 10 min. Accordingly, the nanorod-like $PbCrO_4$ is grown through three processes: the formation of $PbCrO_4$ crystal nuclei, short nanorod (Fig. S2a) and further growth to the long nanorod (Fig. S2b), where the surface energy could be the mainly driving force for the formation of nanorod. The Brunauer-Emmett-Teller (BET) surface area and pore size of the $PbCrO_4$ nanorods are characterized using a N_2 adsorption–desorption isotherm, as shown in Fig. S3. The isotherm is type-III with an H4-type hysteresis loop, indicating a macroporous structure mainly caused by the stacking of the $PbCrO_4$ nanorods [20–22]. The BET surface area is 8.50 $m^2 g^{-1}$. The high-resolution XPS spectra of Pb 4f and Cr 2p are shown in Fig. S4. The binding energies at 142.9, 138.2, 588.1 and 578.9 eV are assigned to Pb $4f_{5/2}$, Pb $4f_{7/2}$, Cr $2p_{1/2}$ and Cr $2p_{3/2}$, respectively, which is in agreement with the reported binding energy values of $PbCrO_4$ [23,24].

The above results (DRS, SPS and UPS) show that the $PbCrO_4$ nanorods have good visible-light harvesting, photoexcited charge separation, and suitable energy band positions, and they can be used for O_2 evolution by water splitting under visible light. Commonly used electron sacrificial agents, such as $AgNO_3$, $FeCl_3$, $Na_2S_2O_8$ are adopted to evaluate the photocatalytic activity for oxygen production over $PbCrO_4$ nanorods. As shown in Fig. S5, the $PbCrO_4$ nanorods exhibits the highest oxygen production with the rate of 15.70 μmol h^{-1} (λ > 420 nm) under $AgNO_3$ (0.1 mol L^{-1}) as electron sacrificial agents. Fig. 4a shows the O_2 evolution in the $PbCrO_4$ nanorods and $BiVO_4$ synthesized by a liquid-solid reaction according to Kudo's report [8] under visible-light irradiation and the $AgNO_3$ (0.1 mol L^{-1}). The O_2 evolution rate of $PbCrO_4$ is higher than that of the as-synthesized $BiVO_4$. A comparison of the normalized O_2 evolution rates with many other reported visible-light-active photocatalysts is shown in Table S2. Clearly, the photocatalytic performance of the synthesized $PbCrO_4$ nanorods is at the top among many reported visible-light-active photocatalysts (polymer carbon nitride, PDINH

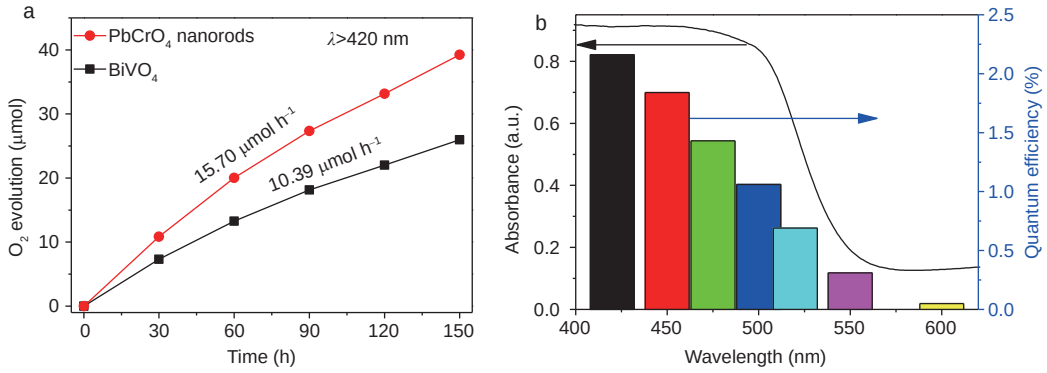

Figure 4 The O_2 evolution of the $PbCrO_4$ nanorods and $BiVO_4$ under visible-light irradiation (a), the measured quantum efficiencies for photons at different wavelengths for the $PbCrO_4$ nanorods (b).

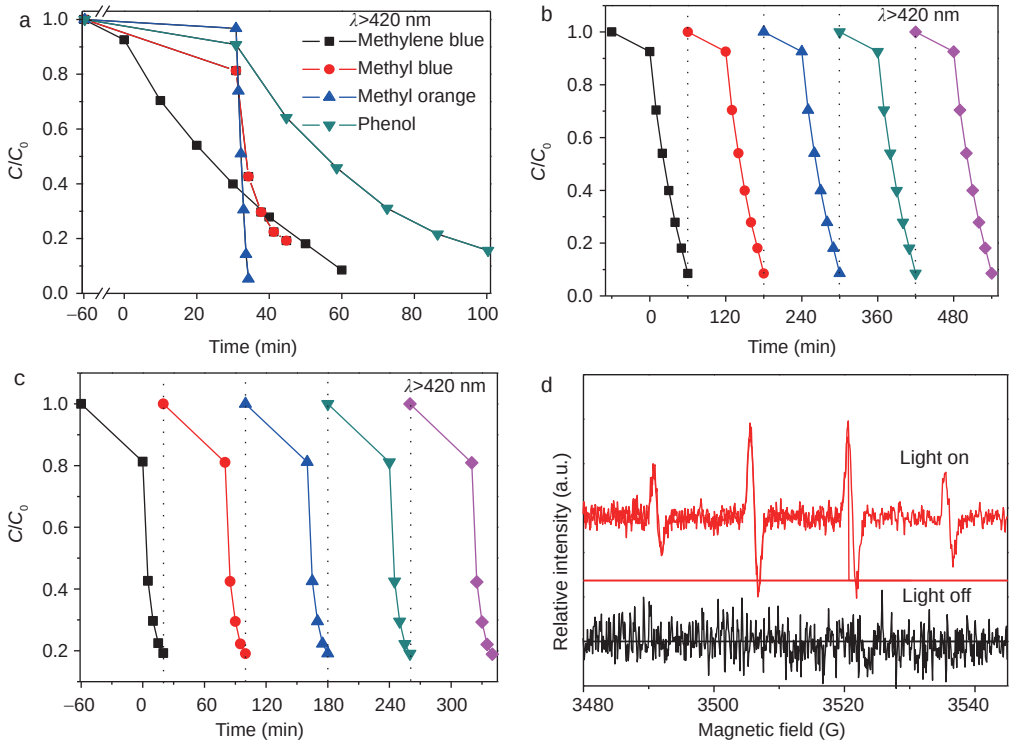

Figure 5 The photocatalytic degradation (λ>420 nm) of dyes (a), recycles measure of photocatalytic degradation of methylene blue (b) and methyl blue (c), the DMPO spin-trapping ESR spectra of $PbCrO_4$ nanorods for ·DMPO-OH (d).

supramolecular, red phosphorus, TaON, Ta_3N_5, $Sm_2Ti_2S_2O_5$, $Sr_{0.9}NbO_3$, Fe_2O_3, $AgPO_4$ and $BiVO_4$). Fig. 4b displays the measured quantum efficiencies for photons at different wavelength for the O_2 evolution reaction over $PbCrO_4$ nanorods. The quantum efficiency is 2.16% and 0.05% at 420±10 and 600±10 nm, respectively.

The photocatalytic decomposition of organics was used to further evaluate the photocatalytic performance of the $PbCrO_4$ nanorods. As shown in Fig. 5a and Figs S7–S10, the $PbCrO_4$ nanorods have excellent photocatalytic degradation performances for methylene blue, methyl blue, methyl orange and phenol. What's more, after five decomposition cycles for methylene blue and methyl blue (Fig. 5b, c), no recession in the photocatalytic activity is observed, indicating the excellent stability of the $PbCrO_4$ nanorods. To clarify the generation of ·OH radicals during the photodegradation reaction, the electron spin resonance (ESR) tests were performed using DMPO spin-trapping, as shown in Fig. 5d. Four characteristic peaks are observed under visible-light irradiation, and the standard ratios of the intensities are 1:2:2:1, which can be ascribed to ·DMPO-OH [25,26]. In contrast, an ESR signal is not detected under dark conditions, indicating that the ·OH radical is the active species during the photocatalytic decomposition. We supplemented the active species trapping experiments to further verify the possible active species in photocatalytic decomposition. The isopropyl alcohol (IPA), ammonium oxalate (AO), and benzoquinone (BQ) were used as scavengers of ·OH, H^+, and $\cdot O_2^-$, respectively in the photocatalytic decomposition of methyl blue [27–29]. As shown in Fig. S11, the photodegradation rates are apparently inhibited by the addition of IPA and AO, while BQ exhibits a relatively weak inhibition. These results suggest that –OH and H^+ are the main active species in the photocatalytic decomposition.

We next investigated the pollution from $PbCrO_4$ by examining the concentrations of Pb^{2+} and Cr^{6+} that dissolved into the water. The solubility product (K_{sp}) of $PbCrO_4$ is 2.8×10^{-13}, and the concentrations of Pb^{2+} and Cr^{6+} are 0.110 and 0.028 ppm, respectively, which are close to the drinking water standard concentrations for Pb^{2+} (0.05 ppm) and Cr^{6+} (0.05 ppm) and lower than the industrial sewage emission standards for Pb^{2+} (1.00 ppm) and Cr^{6+} (1.00 ppm). The inductively coupled plasma optical emission spectrometry (ICP-OES) tests (Table S3) further clarify that Pb and Cr element remain in the reaction solution after the photocatalytic recycling, and the

concentrations are only 0.16±0.02 and 0.00 ppm, respectively. These results show that we can transform heavy-metal Pb(II) and Cr(VI) pollutants into a visible-light-active photocatalyst and produce negligible pollutant residues during the photocatalytic reaction.

CONCLUSIONS

In summary, the $PbCrO_4$ nanorods were successfully developed by a simple precipitation reaction *via* mixing $Pb(NO_3)_2$ and Na_2CrO_4 solutions at room temperature. The obtained nanorods are visible-light-active photocatalyst for high-efficiency photocatalytic O_2 evolution from water and photocatalytic organic pollutants degradation. This simple synthetic method can transform heavy-metal Pb(II) and Cr(VI) pollutants into low toxic $PbCrO_4$ photocatalyst with a narrow band gap of 2.12 eV, excellent stability and high photocatalytic performance and produce negligible pollutant residues during the photocatalytic reaction. This novel photocatalyst may result in the breakthrough in the overall water-splitting reaction, degradation of pollutants and the reuse of Pb(II) and Cr(VI) pollutants.

Received 9 December 2017; accepted 9 February 2018; published online 15 March 2018

1 Chen X, Shen S, Guo L, *et al.* Semiconductor-based photocatalytic hydrogen generation. Chem Rev, 2010, 110: 6503–6570
2 Han T, Chen Y, Tian G, *et al.* Hydrogenated TiO_2/$SrTiO_3$ porous microspheres with tunable band structure for solar-light photocatalytic H_2 and O_2 evolution. Sci China Mater, 2016, 59: 1003–1016
3 Hao R, Jiang B, Li M, *et al.* Fabrication of mixed-crystalline-phase spindle-like TiO_2 for enhanced photocatalytic hydrogen production. Sci China Mater, 2015, 58: 363–369
4 Maeda K, Lu D, Domen K. Solar-driven Z-scheme water splitting using modified $BaZrO_3$–$BaTaO_2N$ solid solutions as photocatalysts. ACS Catal, 2013, 3: 1026–1033
5 Pendlebury SR, Barroso M, Cowan AJ, *et al.* Dynamics of photogenerated holes in nanocrystalline α-Fe_2O_3 electrodes for water oxidation probed by transient absorption spectroscopy. Chem Commun, 2011, 47: 716–718
6 Maeda K, Domen K. Photocatalytic water splitting: recent progress and future challenges. J Phys Chem Lett, 2010, 1: 2655–2661
7 Martin DJ, Umezawa N, Chen X, *et al.* Facet engineered Ag_3PO_4 for efficient water photooxidation. Energy Environ Sci, 2013, 6: 3380–3386
8 Kudo A, Omori K, Kato H. A novel aqueous process for preparation of crystal form-controlled and highly crystalline $BiVO_4$ powder from layered vanadates at room temperature and its photocatalytic and photophysical properties. J Am Chem Soc, 1999, 121: 11459–11467
9 Huang Y, Yu Y, Xin Y, *et al.* Promoting charge carrier utilization by integrating layered double hydroxide nanosheet arrays with porous $BiVO_4$ photoanode for efficient photoelectrochemical water splitting. Sci China Mater, 2017, 60: 193–207
10 Yi Z, Ye J, Kikugawa N, *et al.* An orthophosphate semiconductor with photooxidation properties under visible-light irradiation. Nat Mater, 2010, 9: 559–564
11 Bi Y, Hu H, Ouyang S, *et al.* Photocatalytic and photoelectric properties of cubic Ag_3PO_4 sub-microcrystals with sharp corners and edges. Chem Commun, 2012, 48: 3748–3750
12 Hitoki G, Takata T, Kondo JN, *et al.* An oxynitride, TaON, as an efficient water oxidation photocatalyst under visible light irradiation ($\lambda \leq 500$ nm). Chem Commun, 2002, 86: 1698–1699
13 Chen S, Shen S, Liu G, *et al.* Interface engineering of a CoO_x/Ta_3N_5 photocatalyst for unprecedented water oxidation performance under visible-light-irradiation. Angew Chem Int Ed, 2015, 54: 3047–3051
14 Zhu J, Yin Z, Yang D, *et al.* Hierarchical hollow spheres composed of ultrathin Fe_2O_3 nanosheets for lithium storage and photocatalytic water oxidation. Energy Environ Sci, 2013, 6: 987–993
15 Chen D, Ye J. Hierarchical WO_3 hollow shells: dendrite, sphere, dumbbell, and their photocatalytic properties. Adv Funct Mater, 2010, 18: 1922–1928
16 Monico L, Janssens K, Miliani C, *et al.* Degradation process of lead chromate in paintings by vincent van gogh studied by means of spectromicroscopic methods. 3. Synthesis, characterization, and detection of different crystal forms of the chrome yellow pigment. Anal Chem, 2013, 85: 851–859
17 Burgio L, Melessanaki K, Doulgeridis M, *et al.* Pigment identification in paintings employing laser induced breakdown spectroscopy and Raman microscopy. SpectroChim Acta Part B-Atomic Spectr, 2001, 56: 905–913
18 Cao L, Fei X, Zhao H. Environmental substitution for $PbCrO_4$ pigment with inorganic-organic hybrid pigment. Dyes Pigments, 2017, 142: 100–107
19 Kronik L, Shapira Y. Surface photovoltage phenomena: theory, experiment, and applications. Surf Sci Rep, 1999, 37: 1–206
20 Liu D, Yao Y, Tang D, *et al.* Coal reservoir characteristics and coalbed methane resource assessment in Huainan and Huaibei coalfields, Southern North China. Int J CoalGeol, 2009, 79: 97–112
21 Khalfaoui M, Knani S, Hachicha MA, *et al.* New theoretical expressions for the five adsorption type isotherms classified by BET based on statistical physics treatment. J Colloid Interface Sci, 2003, 263: 350–356
22 Wang J, Yang X, Wu D, *et al.* The porous structures of activated carbon aerogels and their effects on electrochemical performance. J Power Sources, 2008, 185: 589–594
23 Biesinger MC, Brown C, Mycroft JR, *et al.* X-ray photoelectron spectroscopy studies of chromium compounds. Surf Interface Anal, 2004, 36: 1550–1563
24 Parhi P, Manivannan V. Novel microwave initiated synthesis of Zn_2SiO_4 and $MCrO_4$ (M=Ca, Sr, Ba, Pb). J Alloys Compd, 2009, 469: 558–564
25 Li R, Weng Y, Zhou X, *et al.* Achieving overall water splitting using titanium dioxide-based photocatalysts of different phases. Energy Environ Sci, 2015, 8: 2377–2382
26 Xiao X, Jiang J, Zhang L. Selective oxidation of benzyl alcohol into benzaldehyde over semiconductors under visible light: The case of $Bi_{12}O_{17}Cl_2$ nanobelts. Appl Catal B-Environ, 2013, 142-143: 487–493
27 He L, Tong Z, Wang Z, *et al.* Effects of calcination temperature and heating rate on the photocatalytic properties of ZnO prepared by pyrolysis. J Colloid Interface Sci, 2018, 509: 448–456

28 Jiang H, Li M, Liu J, *et al.* Alkali-free synthesis of a novel heterostructured CeO_2-TiO_2 nanocomposite with high performance to reduce Cr(VI) under visible light. Ceramics Int, 2018, 44: 2709–2717
29 Huang H, Huang N, Wang Z, *et al.* Room-temperature synthesis of carnation-like ZnO@AgI hierarchical nanostructures assembled by AgI nanoparticles-decorated ZnO nanosheets with enhanced visible light photocatalytic activity. J Colloid Interface Sci, 2017, 502: 77–88

Acknowledgements This work was jointly supported by the National Natural Science Foundation of China (21401190), the Science and Technology Project of Research Foundation of China Postdoctoral Science (2017M612710 and 2016M592519), Shenzhen Peacock Plan (827-000059, 827-000113 and KQTD2016053112042971), the Science and Technology Planning Project of Guangdong Province (2016B050501005), and the Educational Commission of Guangdong Province (2016KCXTD006 and 2016KSTCX126).

Author contributions Zhang GQ performed the experiments and wrote the manuscript with the guidance from Su CL and Sun X. All authors contributed to the general discussion and revision.

Conflict of interest The authors declare no conflict of interest.

Supplementary information Supporting information is available in the online version of the paper.

Guo-Qiang Zhang received his bachelor degree majored in material chemistry from Lanzhou University in 2012. Then he completed his PhD degree at the University of Chinese Academy of Sciences under the supervision of Prof. Da-Bing Li. His research interest is the semiconductor photocatalytic water spliting. Now, he continues his research on photocatalysis at SZU-NUS International Collaborative Laboratory as a Post-doctor.

Chen-Liang Su received his BSc degree (2005) and PhD degree (2010) in the Department of Chemistry from Zhejiang University (2010). After that he worked as a research fellow at the Advanced 2D Materials and Graphene Research Centre in the National University of Singapore (2010–2015). He is now a full-professor at the International Collaborative Laboratory of 2D Materials for Optoelectronics Science and Technology (ICL-2D MOST), Shenzhen University and a Principal Investigator of ICL-2D MOST in materials science. His current interests focus on the chemical design of 2D materials/nano materials for catalysis and energy related applications.

铬酸铅纳米棒: 一种高效、稳定的可见光产氧和光降解催化剂

张国强[1], 刘国帅[2], 徐杨森[1], 杨建华[3], 李瑛[1], 孙晓娟[4*], 陈伟[5], 苏陈良[1*]

摘要 本文利用简单的沉淀反应将工业废水中含有的剧毒Pb(II)和Cr(VI)离子制备成纳米棒状的黄色颜料$PbCrO_4$. 合成的$PbCrO_4$纳米棒是一种高效的可见光活性产氧和光降解催化剂. 此纳米棒具有优异的光催化稳定性和催化活性, 在可见光下分解水产氧速率高达314.0 μmol h^{-1} g^{-1}, 在420±10 和600±10 nm处量子效率分别为2.16%和0.05%. 此外, 该催化剂还具有良好的可见光降解亚甲基蓝、甲基蓝、甲基橙和苯酚的性能. 以上结果表明, 将剧毒含重金属污染物Pb(II)和Cr(VI)的离子溶液转化为环境友好且高效的可见光光催化剂是可行的. 该策略利用污染物产生清洁能源并降解污染物, 是绿色、环境友好且非常有前景的废物利用途径.

